Selective trapping of positrons by Ag nanolayers in a V/Ag multilayer system

Cite as: AIP Advances **10**, 035012 (2020); https://doi.org/10.1063/1.5143379
Submitted: 23 December 2019 • Accepted: 20 February 2020 • Published Online: 11 March 2020

N. Qi, H. X. Zhang, Z. Q. Chen, et al.

Selective trapping of positrons by Ag nanolayers in a V/Ag multilayer system

Cite as: AIP Advances 10, 035012 (2020); doi: 10.1063/1.5143379
Submitted: 23 December 2019 • Accepted: 20 February 2020 •
Published Online: 11 March 2020

N. Qi,[1] H. X. Zhang,[1] Z. Q. Chen,[1] F. Ren,[1,a)] B. Zhao,[2] M. Jiang,[3,a)] and A. Uedono[4]

AFFILIATIONS

[1]Hubei Nuclear Solid Physics Key Laboratory, Department of Physics, Wuhan University, Wuhan 430072, People's Republic of China
[2]School of Science, Zhongyuan University of Technology, Zhengzhou 450007, People's Republic of China
[3]Department of Nuclear Engineering and Technology, School of Energy and Power Engineering, Huazhong University of Science and Technology, Wuhan 430074, People's Republic of China
[4]Division of Applied Physics, Faculty of Pure and Applied Science, University of Tsukuba, Tsukuba, Ibaraki 305-8573, Japan

[a)]**Authors to whom correspondence should be addressed:** fren@whu.edu.cn and jiangm@hust.edu.cn

ABSTRACT

V/Ag nano-scaled multilayers were prepared by using a magnetron sputtering deposition method. Each layer of Ag and V has a thickness of about 6 nm, and the total thickness of the multilayer film is 350 nm. Doppler broadening of annihilation radiation was measured by using a slow positron beam to study the microstructure of the above samples. It was found that the Doppler broadening S and W parameters measured in the V/Ag multilayers were close to those measured in the Ag reference sample. Coincidence Doppler broadening measurements also showed that the electron momentum distributions in V/Ag multilayers and Ag monolayer were almost identical. This suggests that Ag has a strong affinity to positrons, and almost all the positrons ejected into the multilayers are confined to the Ag nanolayers. Theoretical calculations indicate that the positron wavefunction is well localized in the Ag nanolayer even for a layer thickness of only 1 nm.

I. INTRODUCTION

Nuclear energy has become more and more important in the energy constituents of the future world. However, the materials in nuclear reactors are always subjected to severe irradiation by various energetic particles such as neutrons, α particles, and other fragments generated in fission and fussion nuclear reactions. The collision of these high energy particles with target atoms produces a large number of vacancies and interstitials, and these defects further agglomerate to form dislocation loops, stacking-fault tetrahedra, and even cavities.[1] The interaction of helium with defects such as dislocations, voids, or grain boundaries also leads to the generation of helium bubbles.[2,3] Therefore, the long-term irradiation causes swelling and embrittlement as well as irradiation hardening of materials, which leads to the degradation of the performance of materials and affects the safety of nuclear reactors. The design of novel materials with superior irradiation resistance has become an urgent project.

It was revealed that grain and interphase boundary can be effective sinks for point defects introduced by irradiation and, thus, significantly improve irradiation tolerance of materials.[4–12] Nanocrystalline materials contain large amounts of grain boundaries, which are good candidates as irradiation resistive materials in nuclear reactors. These boundaries are supposed to enhance the recombination of vacancies and interstitials introduced by irradiation.[8] The smaller the grain size, the larger the volume fraction of grain boundary and, thus, the better the irradiation resistance. Therefore, one way to improve the irradiation tolerance of materials is to decrease the grain sizes. This has been verified in various metals such as Fe, Ni, and Au after grain refinement.[5,10,13] However, for these pure metals, the nanograins grow substantially during irradiation. Therefore, the grain boundaries decrease, which deteriorates the irradiation tolerance. The interphase boundaries in immiscible nanocomposites should be a better solution, since the interfaces may remain unaffected during irradiation.

The metallic nano-scaled multilayer system has a large proportion of the interface structure that can absorb defects and favor the defect recovery, and the immiscible interfaces remain stable during irradiation.[14] It is, therefore, an ideal candidate for nuclear reactors, which has high irradiation tolerance. The most frequently studied system is the Cu–Nb multilayers,[7,14–20] which have fcc-bcc interface structures. The other extensively investigated multilayer systems include Cu/V, V/Ag, Cu/W, Cu/Mo, Fe/W, Al/Nb, etc., which all show excellent irradiation resistance.[21–26]

In order to understand the mechanism of the irradiation resistance of multilayer systems, it is necessary to investigate the microstructural evolution of interfaces during irradiation. Positron annihilation spectroscopy is a powerful tool to study atomic scaled defects in materials.[27,28] It is very sensitive to the irradiation induced defects such as vacancies, dislocations, vacancy clusters, helium bubbles, and voids. This method has several advantages over other defect probes. First, it can detect vacancies on an atomic scale, which is difficult for other methods. Transmission electron microscopy (TEM) has difficulties in detecting point defects such as vacancies and vacancy clusters. Even for helium bubbles, the detection limit of TEM is about 1 nm.[29,30] Second, since a positron is positively charged, it is repelled by the positive ion cores in a perfect lattice. If there is a vacancy, the positron is preferentially trapped at this site. Due to the self-seeking ability of positron, it has outstanding sensitivity to vacancy defects, which is as high as 10^{-7}/atom. Third, positron annihilation is a non-destructive probe, and no complex sample preparation is needed.

The interfacial regions of a multilayer system can be studied using an energy variable slow positron beam,[31] since interfaces are also positron trapping centers. There have been several reports on the study of interfaces using a slow positron beam. Typical examples are SiO_2/Si interface,[32–35] SiO_2/SiC interface,[36,37] and AlO_x/SiO_2/Si interface.[38] It is thus meaningful to study the detailed interaction between defects and interfaces by positron annihilation spectroscopy. However, since the metallic multilayers are composed of two or more different types of metals, the positron affinity of these metals is different.[39] Therefore, positrons prefer to be confined to one type of metals.[40–42] In other words, positrons are trapped by some specific metal layer rather than by the interfaces and, thus, makes the interfaces invisible to positrons. To check this possibility, we prepared V/Ag nano-scaled multilayers by magnetron sputtering and studied the microstructural properties by using a slow positron beam. Our results show clear evidence of positron confinement in Ag nanolayers.

II. EXPERIMENT AND THEORETICAL CALCULATION

The V/Ag multilayers were deposited on Si (100) substrates by using a magnetron sputtering system (ULVAC, ACS-4000-C4). V and Ag nanolayers were deposited alternatively. The vacuum chamber was first evacuated to a base pressure of better than 5×10^{-6} Pa, then the deposition was performed with a working pressure of 0.5 Pa. The working gas was Ar and the distance between the target and substrate was kept at 130 mm. Prior to deposition of V/Ag multilayers, a 10 nm thick V layer was deposited as a buffer layer, and the top layer was also a V layer to avoid oxidation. Pure Ag and V layers were also deposited on Si substrates as reference samples.

The microstructure of the pure V, Ag layers, and V/Ag multilayers was studied by TEM [JEOL JEM-2010(HT), 200 kV] and scanning electron microscopy (SEM) (FEI SIRION, 25 kV). A slow positron beam was also used to study the microstructure of V/Ag layers. The positron energy varies from 0.1 keV to 30 keV. Doppler broadening spectra of the annihilation radiation were measured as a function of the incident positron energy using a high purity Ge detector with an energy resolution of about 1.18 keV at 511 keV. The recorded spectra were analyzed by the conventional S and W parameters, which are defined as the relative number of annihilation events in the central region (511 ± 0.76 keV) and wing region (511 ± 3.4 keV to 511 ± 6.8 keV), respectively. Coincidence Doppler broadening (CDB) spectra were also measured at some selected positron energies using two Ge detectors in opposite directions. Each CDB spectrum contains a total count of about 5×10^6.

Theoretical calculation of positron density in the multilayer system is performed using the standard atomic superposition (ATSUP) method.[43] To solve the needed electron and positron densities, we used the conventional scheme of the two-component density-functional theory, based on the well-established Boronski–Nieminen parametrization, to calculate the positron–electron correlation potential as well as the enhancement factor of positron annihilation.[44] The positron wave function at the point (k = 0) was obtained by solving the positron Kohn–Sham equation in reciprocal space by using the numerical diagonalization technique.

III. RESULTS AND DISCUSSION

Figure 1 shows the cross-sectional scanning electron microscopy (SEM) images of pure V and Ag layers grown on Si substrates. It can be seen that the Ag layer shows a layered growth, while the V layer shows a columnar growth.[45] This is in agreement with the previous results observed by Wei *et al.*[22,46] The thickness for both pure V and Ag layers was about 500 nm. Figure 2 shows the bright field TEM image of the V/Ag multilayer. The TEM image confirms the formation of multilayer structures with sharp interfaces. The layers with bright contrast are V layers, while the layers with dark contrast are Ag layers. Each V layer and Ag layer has an equal thickness of about 6 nm. About 30 layers of V and 30 layers of Ag were deposited, and the total thickness of the V/Ag multilayers is about 350 nm. The top layer is ended by a V layer. Due to the ultrathin layer of V and Ag, the tendency of the columnar growth of V layers is suppressed.[45]

Figure 3 shows the S and W parameters as a function of incident positron energy E (called S–E and W–E curves) measured for the

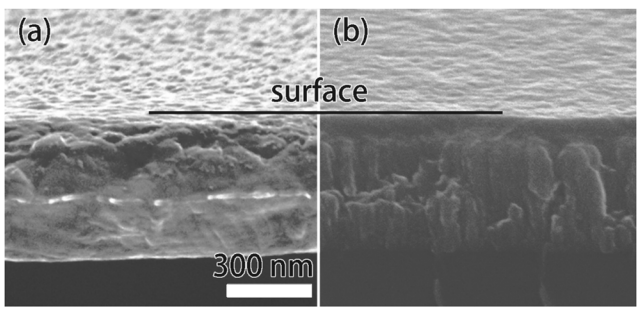

FIG. 1. Cross-sectional SEM image of (a) pure Ag layer and (b) pure V layer.

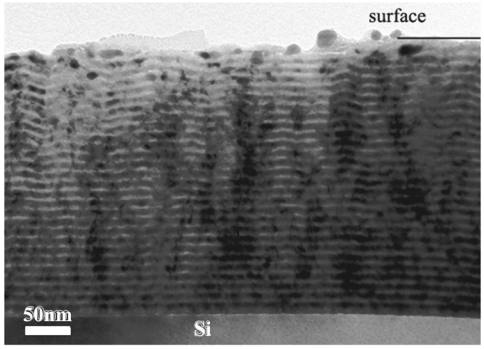

FIG. 2. Cross-sectional TEM images of V/Ag multilayers. Each V and Ag layer has a thickness of about 6 nm.

pure V layer, pure Ag layer, and V/Ag multilayers. For pure Ag layer, the S parameter starts with a value of about 0.490, then it decreases with increasing positron energy up to about 6 keV. This is due to the decrease of the chance of positron diffusing back to the surface. Between 6 keV and 11 keV, the S parameter declines very slightly. This means that almost all the incident positrons annihilated in the deep Ag layer without returning back to the surface. In other words, due to a higher incident energy, positrons are implanted into deeper regions, which makes them difficult to diffuse back to the surface. Therefore, it is reasonable to deduce that the energy range of 6–11 keV corresponds to positron annihilating in the Ag layer. When the positron energy increases to above 11 keV, the S parameter begins to increase. This is due to the fact that more positrons are ejected into the Si substrate when the positron energy is higher than 11 keV, and the S parameter in Si is obviously higher than that in the Ag layer.

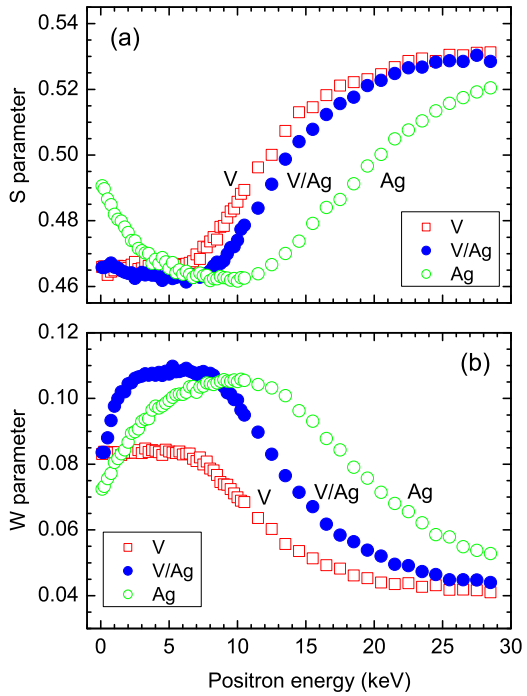

FIG. 3. Doppler broadening (a) S and (b) W parameters as a function of positron energy measured for the pure V layer, pure Ag layer, and V/Ag multilayers.

From the above analysis of the S–E curve for pure Ag layer, one can find that with increasing positron energy, the positrons can detect the surface, Ag layer, and Si substrate, successively. This means that the region sampled by slow positrons can be divided into several layers. Considering the broad implantation profile and also diffusion of positrons, for certain incident energy, the positrons may finally annihilate in different layers. Therefore, at any positron energy E, the measured S parameter is a linear combination of the S parameter in each layer,

$$S(E) = S_S F_S(E) + \sum_{i=1}^{n} S_i F_i(E), \tag{1}$$

$$F_S(E) + \sum_{i=1}^{n} F_i(E) = 1, \tag{2}$$

where S_S and S_i are the S parameters at the surface and in the i-th layer, respectively. The S parameter is assumed to be approximately the same within each layer. The measured S–E curve is then analyzed by using the VEPFIT program[47] by solving the following one-dimensional diffusion equation:

$$D_+ \frac{d^2}{dz^2} n(z) - \kappa_{eff}(z) n(z) + P(z, E) = 0, \tag{3}$$

where $n(z)$ is the positron density at distance z from the surface, $P(z, E)$ is the positron implantation profile at a given energy E, $\kappa_{eff}(z)$ is the effective escape rate of positrons from the diffusion process, and D_+ is the positron diffusion coefficient.

The positron implantation profile can be well approximated by the Makhov equation, which is adopted in the VEPFIT analysis,

$$P(z, E) = \frac{m z^{m-1}}{z_0^m} \exp\left[-\left(\frac{z}{z_0}\right)^m\right], \tag{4}$$

where $z_0 = \bar{z}/\Gamma(1 + \frac{1}{m})$, Γ is the gamma function, $\bar{z}$ is the mean implantation depth of positrons, which can be estimated by the following equation:

$$\bar{z} = AE^n/\rho. \tag{5}$$

Here, m, n, and A are constants, and ρ is the material density. Generally, the values of m, n, and A are 2.0, 1.6, and 4×10^{-6} g cm^{-2} keV$^{-1.6}$, respectively.[47]

According to the VEPFIT analysis, the S parameter in the Ag layer is about 0.462. This is just the S value between 6 keV and 11 keV in the S–E curve of the pure Ag layer. Therefore, it confirms that the flat region of the S–E curve between 6 keV and 11 keV can be attributed to positron annihilation in the Ag layer. The fitted S parameter in the Si substrate is about 0.535, which is also in agreement with the S value we measure for Si single crystals. The Ag layer thickness from fitting is about 413 ± 25 nm, rather closed to the thickness obtained by SEM measurements. For the pure V layer, the S parameter remains almost constant in the energy range of 0.1–7 keV. Above this region, it begins to increase and finally reaches the S value level for the Si substrate. It seems that the S parameter of the surface state is close to that in the V layer, so we have not observed the shift of positron from the surface state to the deep bulk

state. Thus, we do believe that the S parameter in the energy range of 0.1–7 keV corresponds to the positron annihilation in the V layer. The S parameter in the V layer is about 0.465 from the VEPFIT fitting. The upper limit of the positron incident energy in the V layer is much lower than that of the Ag layer. This is due to different densities of these two metals. Ag has a higher density of 10.49 g/cm^3; therefore, a higher positron energy is needed to reach the same depth as in the V layer, which has a lower density of 6.11 g/cm^3. For the V/Ag multilayers, the S–E curve resembles that of the pure V layer. The S parameter at the surface state is around 0.466, which is close to that of the V layer. This is because that the top layer of the V/Ag multilayers is terminated by the V nanolayer. The S parameter shows a slight decrease with an increase in the positron energy of up to 2 keV, and then, it remains constant in the energy range of 2–8 keV, due to the positron annihilation in V/Ag multilayers. The S parameter in the multilayers is about 0.463.

The S parameters for pure V layer, pure Ag layer, and V/Ag multilayers are very close to each other, and the S–E curve for V/Ag multilayers looks like that of the V layer. This might cause a misunderstanding of the results, it seems that positrons prefer to stay inside the V layers in the multilayer system so that the S–E curve is similar to that of the V layer. However, we can further check the W–E curves for these three samples as shown in Fig. 3(b). For V/Ag multilayers, the W parameter near the surface stays still the same as that of the V layer. However, the whole W–E curve for V/Ag multilayers is different from that of the V layer. Instead, it is closer to that of the Ag layer. Especially, the W parameter in the V/Ag multilayers (2–8 keV) is very close to that of the Ag layer (6–11 keV). The individual S and W parameters for these three samples are summarized in Table I. It is clear that both S and W parameters for V/Ag multilayers remain almost the same as those in the pure Ag layer.

The variation of parameters S vs W (S–W curve) with increasing positron energy for each sample can give more complementary information on the positron annihilation behavior. Figure 4 shows the S–W curves for these three samples. For the pure V layer, the S–W curve can be fitted by a straight line, and with increasing positron energy, the S–W data move from the V layer to the Si substrate. The surface state is indistinguishable from the bulk state of V. For the pure Ag layer, the S–W curve can be fitted by two different lines. The S–W data start from the surface state at (0.4906, 0.0725), and move toward the (S, W) value of Ag (0.465, 0.105), then move to the Si substrate (0.535, 0.04). As for the V/Ag multilayers, one can use two lines to fit the S–W data. The S–W curve starts from the same surface state of the pure V layer, and with increasing positron energy, it moves to the Ag state, then deflects to the Si substrate. This implies that at an energy range of 2–8 keV when positrons are ejected into the V/Ag multilayers, the positrons prefer to stay at Ag nanolayers and annihilation also happen there.

TABLE I. Doppler broadening S and W parameters in pure V film, pure Ag film, and V/Ag multilayers.

Sample	S parameter	W parameter
V film	0.465 ± 0.001	0.0835 ± 0.0004
Ag film	0.462 ± 0.001	0.1054 ± 0.0004
V/Ag multilayer	0.463 ± 0.001	0.1075 ± 0.0004

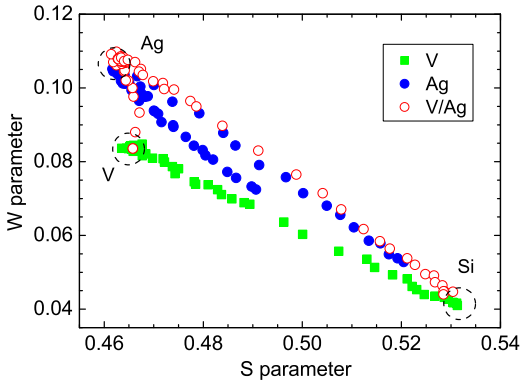

FIG. 4. Change of S vs W parameters with increasing incident positron energy measured for the pure V layer, pure Ag layer, and V/Ag multilayers.

For the incident positron energy in the range of 2–8 keV, all the positrons are ejected in the Ag nanolayers and annihilate therein. This possibility, however, is extremely small, since positrons have a broad implantation profile. We calculated the positron stopping profile in pure V and Ag with an incident energy of 2 keV, 5 keV, 10 keV, and 15 keV by using the Makhov equation in Eq. (4). The results are plotted in Fig. 5. It can be seen that for a medium energy of 5 keV, the positron implantation profile covers a depth range of more than 100 nm for either V or Ag layer, which is almost 20 nanolayers. This means that even for positrons with the same incident energy, they are distributed in both V and Ag nanolayers. The same annihilation S and W parameters in V/Ag multilayers as those in the pure Ag

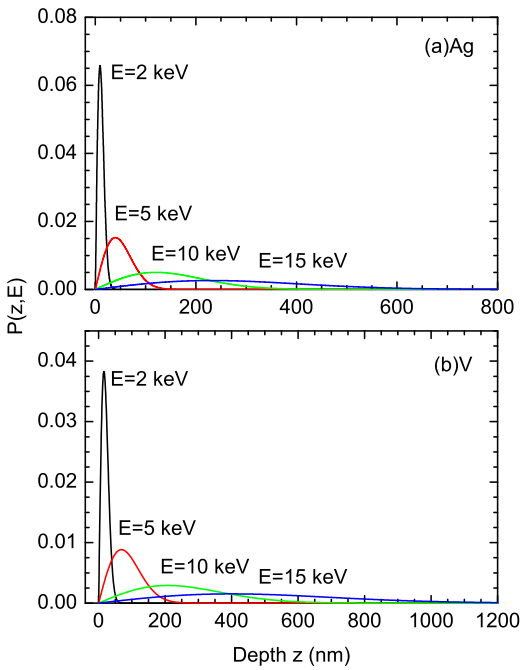

FIG. 5. Positron implantation profiles at selected energies in (a) Ag and (b) V calculated using the Makhov equation.

layer just implies that positrons may get trapped in Ag nanolayers even when they are ejected in V nanolayers.

To confirm the positron trapping by Ag nanolayers, we also measured the coincidence Doppler broadening (CDB) spectra for the pure V layer, the pure Ag layer, and the V/Ag multilayers. The positron incident energies for these three samples are chosen to be 5 keV, 10 keV, and 6 keV, respectively. Figure 6 shows the CDB spectra. It can be seen that the CDB curve of V/Ag multilayers completely overlaps with that of the pure Ag layer, while diverging from that of the pure V layer. In order to magnify this difference, we calculated the ratio curve of the CDB spectra. The reference sample is a pure V layer. As can be seen in Fig. 7, the CDB ratio curve of the pure Ag layer with respect to the pure V layer has a broad peak in the high momentum region. The center of this peak is around 15×10^{-3} m_0c. For V/Ag multilayers, the CDB ratio curve shows a similar broad peak, indicating that almost all the positrons are confined to the Ag nanolayers.

It has been revealed that positrons can be trapped by quantum-dots like nanoclusters, such as solute clusters in alloys,[40] due to stronger affinity of the solute atom than that of the host atom. In the multilayer sample, the positron affinity for Ag is about −5.36 eV, which is much stronger than that of V (−3.44 eV).[39] According to the theoretical prediction, the minimum radius of nanoclusters that trap positrons can be estimated by the following formula:[39]

$$r(\text{Å}) = \frac{3.1}{\sqrt{\Delta A_+(\text{eV})}}, \tag{6}$$

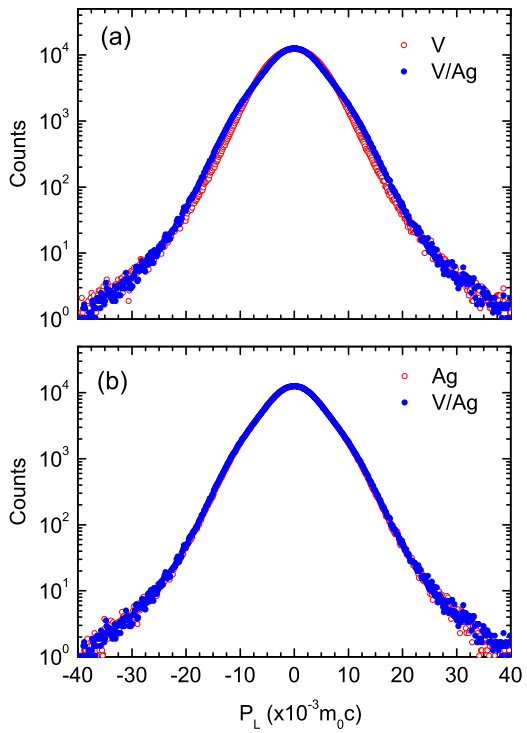

FIG. 6. CDB spectra measured for (a) pure V layer and V/Ag multilayers and (b) pure Ag layer and V/Ag multilayers.

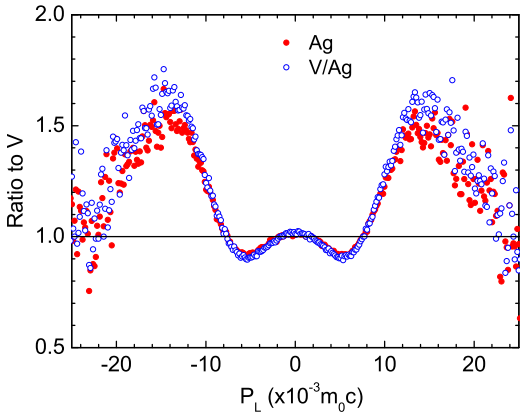

FIG. 7. Ratio curve of the CDB spectra measured for the pure Ag layer and V/Ag multilayers with respect to the pure V layer.

where ΔA_+ is the difference of positron affinities between the solute atom and the host atom. As for the V/Ag multilayers, ΔA_+ is about 1.92 eV, so the minimum diameter for Ag clusters to trap positrons is about 0.9 nm. For a layered structure, the minimum thickness for Ag nanolayers to trap positrons should be around 0.9 nm or even smaller. Since the Ag nanolayer thickness is about 6 nm in this study, it is thick enough to trap positrons. As long as the positron diffusion length in V is longer than the V nanolayer thickness (6 nm), it can diffuse to the adjacent Ag nanolayers and get trapped there.

In order to further verify the positron locations in Ag nanolayers, we calculated the positron wavefunction in the V/Ag multilayers. We constructed an ideal V/Ag multilayer structure with one Ag layer sandwiched between two V layers. The thickness of the Ag layer is about 1 nm, which is close to the minimum size of Ag clusters to trap positrons according to Eq. (6). Figure 8 shows the constructed V–Ag–V layered structure and the calculated positron wavefunction. One can find that the positrons are well localized in the Ag layer, and the positron density in the V layer is almost negligible. The lifetime of positrons trapped in the Ag layer was also calculated, which is presented in Table II together with that in pure V and Ag. For pure V and Ag, the calculated positron lifetimes are 115.5 ps and 123.7 ps, respectively, which are very close to the values of 115 ps and 124 ps calculated by others.[48,49] The experimental values of the positron lifetime in V and Ag are 130 ps and 133 ps, respectively.[50,51] There is a small difference between the theoretical and experiment values. However, it is clear that the positron lifetime in V is shorter than that in Ag. For the constructed V–Ag–V multilayers, the calculated positron lifetime is about 124 ps, which is almost the same as that in pure Ag. Therefore, our calculation confirms that positrons can be selectively trapped by the Ag layer even though the thickness is as small as 1 nm.

Since it is the interfaces in the multilayer system that plays an important role in enhancing irradiation resistance, more attention should be paid to the interface engineering. However, in the present V/Ag multilayers, no interface is detected by the energy variable slow positron beam. This is apparently due to the selective trapping of positrons by Ag nanolayers; thus, the interfaces between Ag and V layers become invisible to positrons. There is another possibility, i.e., the interfaces might not be an effective trapping center for

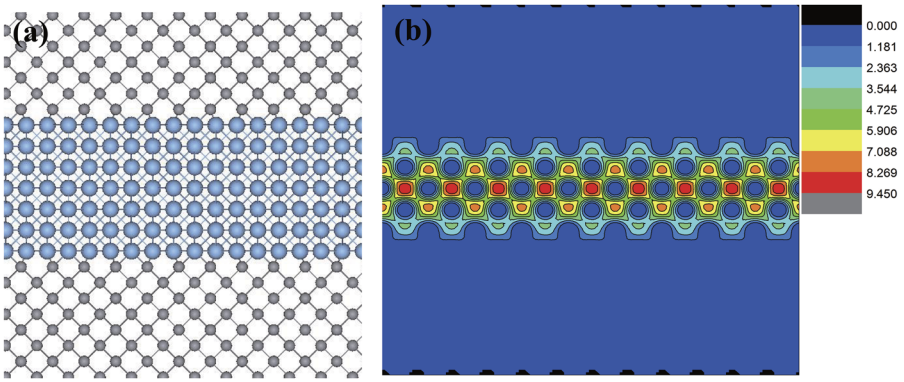

FIG. 8. (a) Constructed V–Ag–V three layer structure (gray and blue spheres represent V and Ag atoms, respectively); (b) positron wave function in the V–Ag–V multilayer.

TABLE II. Calculated positron lifetime in pure V, pure Ag, and V/Ag multilayers.

Sample	Our calculation (ps)	Previous (ps)	Expt. (ps)
V	115.5	115[48,49]	130[50]
Ag	123.7	124[48,49]	133[51]
V/Ag	124.7	...	...

positrons. A deliberate design of the sample structure is needed to check whether interfaces can be detected by positrons. For example, it is desirable to fabricate multilayers in which the individual metal layer has similar positron affinity, so the interfaces can be a trapping center of position. It is also worthwhile to vary the periods of the multilayers to check the competition among interfaces and individual nanolayers, such as the Ag layer in the V/Ag system.

IV. CONCLUSION

The microstructure of V/Ag multilayers was studied by positron annihilation spectroscopy using a slow positron beam. Doppler broadening S and W parameters measured in V/Ag multilayers were very close to those measured in a pure Ag layer, suggesting that positrons preferentially get trapped in Ag nanolayers. Furthermore, coincidence Doppler broadening spectra and the ratio curve measurements for V/Ag multilayers coincide well with those for a pure Ag layer. The results suggested that Ag nanolayers have a stronger ability than an interface to trap positrons. Further work about the effect of the V/Ag layer thickness on the confinement of positrons is under consideration.

ACKNOWLEDGMENTS

This work was supported by the National Key R&D Program of China (Grant No. 2019YFA0210003) and the National Natural Science Foundation of China under Grant Nos. 11875208, 11605232, and 11775163.

DATA AVAILABILITY

The data that support the findings of this study are available from the corresponding author upon reasonable request.

REFERENCES

[1] S. Was Gary, *Fundamentals of Radiation Materials Science* (Springer, New York, 2007).
[2] K. Ono, K. Arakawa, M. Oohashi, H. Kurata, K. Hojou, and N. Yoshida, "Formation and migration of helium bubbles in Fe–16Cr–17Ni austenitic alloy at high temperature," J. Nucl. Mater. **283-287**, 210–214 (2000).
[3] I. I. Chernov, A. N. Kalashnikov, B. A. Kalin, and S. Y. Binyukova, "Gas bubbles evolution peculiarities in ferritic–martensitic and austenitic steels and alloys under helium-ion irradiation," J. Nucl. Mater. **323**(2), 341–345 (2003).
[4] M. Samaras, P. M. Derlet, H. Van Swygenhoven, and M. Victoria, "Computer simulation of displacement cascades in nanocrystalline Ni," Phys. Rev. Lett. **88**, 125505 (2002).
[5] N. Nita, R. Schaeublin, and M. Victoria, "Impact of irradiation on the microstructure of nanocrystalline materials," J. Nucl. Mater. **329-333**, 953–957 (2004).
[6] T. D. Shen, S. Feng, M. Tang, J. A. Valdez, Y. Wang, and K. E. Sickafus, "Enhanced radiation tolerance in nanocrystalline $MgGa_2O_4$," Appl. Phys. Lett. **90**(26), 263115 (2007).
[7] M. J. Demkowicz, R. G. Hoagland, and J. P. Hirth, "Interface structure and radiation damage resistance in Cu-Nb multilayer nanocomposites," Phys. Rev. Lett. **100**, 136102 (2008).
[8] X. M. Bai, A. F. Voter, R. G. Hoagland, M. Nastasi, and B. P. Uberuaga, "Efficient annealing of radiation damage near grain boundaries via interstitial emission," Science **327**(5973), 1631–1634 (2010).
[9] C. Sun, K. Y. Yu, J. H. Lee, Y. Liu, H. Wang, L. Shao, S. A. Maloy, K. T. Hartwig, and X. Zhang, "Enhanced radiation tolerance of ultrafine grained Fe–Cr–Ni alloy," J. Nucl. Mater. **420**(1), 235–240 (2012).
[10] K. Y. Yu, Y. Liu, C. Sun, H. Wang, L. Shao, E. G. Fu, and X. Zhang, "Radiation damage in helium ion irradiated nanocrystalline Fe," J. Nucl. Mater. **425**(1), 140–146 (2012).
[11] X. Y. Liu, B. P. Uberuaga, M. J. Demkowicz, T. C. Germann, A. Misra, and M. Nastasi, "Mechanism for recombination of radiation-induced point defects at interphase boundaries," Phys. Rev. B **85**, 012103 (2012).
[12] I. J. Beyerlein, A. Caro, M. J. Demkowicz, N. A. Mara, A. Misra, and B. P. Uberuaga, "Radiation damage tolerant nanomaterials," Mater. Today **16**(11), 443–449 (2013).
[13] Y. Chimi, A. Iwase, N. Ishikawa, M. Kobiyama, T. Inami, T. Kambara, and S. Okuda, "Swift heavy ion irradiation effects in nanocrystalline gold," Nucl. Instrum. Methods Phys. Res., Sect. B **245**(1), 171–175 (2006).
[14] T. Hőchbauer, A. Misra, K. Hattar, and R. G. Hoagland, "Influence of interfaces on the storage of ion-implanted He in multilayered metallic composites," J. Appl. Phys. **98**(12), 123516 (2005).
[15] X. Zhang, N. Li, O. Anderoglu, H. Wang, J. G. Swadener, T. Hőchbauer, A. Misra, and R. G. Hoagland, "Nanostructured Cu/Nb multilayers subjected to helium ion-irradiation," Nucl. Instrum. Methods Phys. Res., Sect. B **261**(1), 1129–1132 (2007).

[16]N. A. Mara, D. Bhattacharyya, J. P. Hirth, P. Dickerson, and A. Misra, "Mechanism for shear banding in nanolayered composites," Appl. Phys. Lett. **97**(2), 021909 (2010).
[17]W. Z. Han, J. S. Carpenter, J. Wang, I. J. Beyerlein, and N. A. Mara, "Atomic-level study of twin nucleation from face-centered-cubic/body-centered-cubic interfaces in nanolamellar composites," Appl. Phys. Lett. **100**(1), 011911 (2012).
[18]M. G. McPhie, L. Capolungo, A. Y. Dunn, and M. Cherkaoui, "Interfacial trapping mechanism of He in Cu–Nb multilayer materials," J. Nucl. Mater. **437**(1), 222–228 (2013).
[19]L. Zhang and M. J. Demkowicz, "Morphological stability of Cu-Nb nanocomposites under high-energy collision cascades," Appl. Phys. Lett. **103**(6), 061604 (2013).
[20]M. Zhernenkov, S. Gill, V. Stanic, E. DiMasi, K. Kisslinger, J. K. Baldwin, A. Misra, M. J. Demkowicz, and L. Ecker, "Design of radiation resistant metallic multilayers for advanced nuclear systems," Appl. Phys. Lett. **104**(24), 241906 (2014).
[21]E. G. Fu, A. Misra, H. Wang, L. Shao, and X. Zhang, "Interface enabled defects reduction in helium ion irradiated Cu/V nanolayers," J. Nucl. Mater. **407**(3), 178–188 (2010).
[22]Q. M. Wei, N. Li, N. Mara, M. Nastasi, and A. Misra, "Suppression of irradiation hardening in nanoscale V/Ag multilayers," Acta Mater. **59**(16), 6331–6340 (2011).
[23]Y. Gao, T. Yang, J. Xue, S. Yan, S. Zhou, Y. Wang, D. T. K. Kwok, P. K. Chu, and Y. Zhang, "Radiation tolerance of Cu/W multilayered nanocomposites," J. Nucl. Mater. **413**(1), 11–15 (2011).
[24]N. Li, M. S. Martin, O. Anderoglu, A. Misra, L. Shao, H. Wang, and X. Zhang, "He ion irradiation damage in Al/Nb multilayers," J. Appl. Phys. **105**(12), 123522 (2009).
[25]N. Li, K. Y. Yu, J. Lee, H. Wang, and X. Zhang, "Size dependent strengthening mechanisms in sputtered Fe/W multilayers," J. Appl. Phys. **107**(9), 093503 (2010).
[26]N. Li, J. J. Carter, A. Misra, L. Shao, H. Wang, and X. Zhang, "The influence of interfaces on the formation of bubbles in He-ion-irradiated Cu/Mo nanolayers," Philos. Mag. Lett. **91**(1), 18–28 (2011).
[27]A. Dupasquier and A. Mills, Jr., *Positron Spectroscopy of Solids* (IOS Press, Amsterdam, 1995), Vol. 125.
[28]R. Krause-Rehberg and H. S. Leipner, *Positron Annihilation in Semiconductors: Defect Studies* (Springer, Berlin, 1999), Vol. 127.
[29]B. Glam, S. Eliezer, D. Moreno, and D. Eliezer, "Helium bubbles formation in aluminum: Bulk diffusion and near-surface diffusion using TEM observations," J. Nucl. Mater. **392**(3), 413–419 (2009).
[30]P. D. Edmondson, C. M. Parish, Y. Zhang, A. Hallén, and M. K. Miller, "Helium bubble distributions in a nanostructured ferritic alloy," J. Nucl. Mater. **434**(1), 210–216 (2013).
[31]P. G. Coleman, *Positron Beams and Their Applications* (World Scientific, 2000).
[32]P. Asoka-Kumar, K. G. Lynn, and D. O. Welch, "Characterization of defects in Si and SiO_2-Si using positrons," J. Appl. Phys. **76**(9), 4935–4982 (1994).
[33]M. Clement, J. M. M. de Nijs, P. Balk, H. Schut, and A. van Veen, "Transport of positrons in the electrically biased metal-oxide-silicon system," J. Appl. Phys. **81**(4), 1943–1955 (1997).
[34]R. Suzuki, T. Ohdaira, A. Uedono, and Y. Kobayashi, "Positron annihilation in SiO_2–Si studied by a pulsed slow positron beam," Appl. Surf. Sci. **194**(1), 89–96 (2002).
[35]G. Brauer, W. Anwand, W. Skorupa, A. G. Revesz, and J. Kuriplach, "Characterization of the SiO_2/Si interface by positron annihilation spectroscopy," Phys. Rev. B **66**, 195331 (2002).
[36]J. Dekker, K. Saarinen, H. Ólafsson, and E. Ö. Sveinbjörnsson, "Observation of interface defects in thermally oxidized SiC using positron annihilation," Appl. Phys. Lett. **82**(13), 2020–2022 (2003).
[37]M. Maekawa, A. Kawasuso, M. Yoshikawa, A. Miyashita, R. Suzuki, and T. Ohdaira, "Structure of SiO_2/4H-SiC interface probed by positron annihilation spectroscopy," Phys. Rev. B **73**, 014111 (2006).
[38]C. J. Edwardson, P. G. Coleman, T.-T. A. Li, A. Cuevas, and S. Ruffell, "Positron annihilation studies of the AlO_x/SiO_2/Si interface in solar cell structures," J. Appl. Phys. **111**(5), 053515 (2012).
[39]M. J. Puska, P. Lanki, and R. M. Nieminen, "Positron affinities for elemental metals," J. Phys.: Condens. Matter **1**(35), 6081 (1989).
[40]Y. Nagai, M. Hasegawa, Z. Tang, A. Hempel, K. Yubuta, T. Shimamura, Y. Kawazoe, A. Kawai, and F. Kano, "Positron confinement in ultrafine embedded particles: Quantum-dot-like state in an Fe-Cu alloy," Phys. Rev. B **61**, 6574–6578 (2000).
[41]C. Hugenschmidt, P. Pikart, M. Stadlbauer, and K. Schreckenbach, "High elemental selectivity to Sn submonolayers embedded in al using positron annihilation spectroscopy," Phys. Rev. B **77**, 092105 (2008).
[42]P. Pikart, C. Hugenschmidt, M. Horisberger, Y. Matsukawa, M. Hatakeyama, T. Toyama, and Y. Nagai, "Positron annihilation in Cr, Cu, and Au layers embedded in Al and quantum confinement of positrons in Au clusters," Phys. Rev. B **84**, 014106 (2011).
[43]M. J. Puska and R. M. Nieminen, "Defect spectroscopy with positrons: A general calculational method," J. Phys. F: Met. Phys. **13**(2), 333 (1983).
[44]M. J. Puska, A. P. Seitsonen, and R. M. Nieminen, "Electron-positron Car-Parrinello methods: Self-consistent treatment of charge densities and ionic relaxations," Phys. Rev. B **52**, 10947–10961 (1995).
[45]H. Zhang, F. Ren, M. Hong, X. Xiao, G. Cai, and C. Jiang, "Structure and growth mechanism of V/Ag multilayers with different periodic thickness fabricated by magnetron sputtering deposition," J. Mater. Sci. Technol. **30**(10), 1012–1019 (2014).
[46]Q. M. Wei, Y. Q. Wang, M. Nastasi, and A. Misra, "Nucleation and growth of bubbles in He ion-implanted V/Ag multilayers," Philos. Mag. **91**(4), 553–573 (2011).
[47]A. v. Veen, H. Schut, J. d. Vries, R. A. Hakvoort, and M. R. Ijpma, "Analysis of positron profiling data by means of "VEPFIT"," AIP Conf. Proc. **218**(1), 171–198 (1991).
[48]H. Takenaka and D. J. Singh, "Full-potential all-electron positron lifetime calculations: Assessment of local enhancement factors," Phys. Rev. B **77**, 155132 (2008).
[49]J. M. C. Robles, E. Ogando, and F. Plazaola, "Positron lifetime calculation for the elements of the periodic table," J. Phys.: Condens. Matter **19**(17), 176222 (2007).
[50]K. O. Jensen, "Local density calculation of positron annihilation in metals," J. Phys.: Condens. Matter **1**(51), 10595 (1989).
[51]D. O. Welch and K. G. Lynn, "Systematic variation of the mean positron lifetime and Gaussian fraction in annealed metals and semiconductors," Phys. Status Solidi B **77**(1), 277–286 (1976).